

Mass conservative lattice Boltzmann scheme for a three-dimensional diffuse interface model with Peng-Robinson equation of state

Zhonghua Qiao,¹ Xuguang Yang,^{1,2,*} and Yuze Zhang¹

¹*Department of Applied Mathematics, The Hong Kong Polytechnic University, Hung Hom, Hong Kong*

²*School of Mathematics and Computational Science, Hunan First Normal University, Changsha, People's Republic of China*



(Received 21 March 2018; revised manuscript received 9 July 2018; published 14 August 2018)

Peng-Robinson (P-R) equation of state (EOS) has been widely used in the petroleum industry for hydrocarbon fluids. In this work, a three-dimensional diffuse interface model with P-R EOS for two-phase fluid system is solved by the lattice Boltzmann (LB) method. In this diffuse interface model, an Allen-Cahn (A-C) type phase equation with strong nonlinear source term is derived. Using the multiscale Chapman-Enskog analysis, the A-C type phase equation can be recovered from the proposed LB method. Besides, a Lagrange multiplier is introduced based on the mesoscopic character of the LB scheme so that total mass of the hydrocarbon system is preserved. Three-dimensional numerical simulations of realistic hydrocarbon components, such as isobutane and propane, are implemented to illustrate the effectiveness of the proposed mass conservative LB scheme. Numerical results reach a better agreement with laboratory data compared to previous results of two-dimensional numerical simulations.

DOI: [10.1103/PhysRevE.98.023306](https://doi.org/10.1103/PhysRevE.98.023306)

I. INTRODUCTION

Multiphase flow systems extensively exist in numerous scientific and industrial applications, such as oil and gas industries [1–3], environmental protection [4,5], and chemical processing. Understanding and modeling multiphase fluid systems play a very important role in solving these applied science and industry problems. The most critical aspect in the simulation of multiphase flow is to predict interfacial properties accurately between different phases.

Generally, there are three approaches to capture the phase interface: molecular simulation or molecular Monte Carlo simulation [6,7], sharp interface method [8–10], and diffuse interface method [11,12]. In this paper, we focus on the diffuse interface modeling of multiphase flow systems. The basic idea of the diffuse interface method is to treat the phase interfaces as transitional regions with nonzero thickness, where the fluid properties vary smoothly across the interfaces. Thus, the interface curvature and the complex interfacial dynamics can be resolved with higher accuracy. The diffuse interface modeling has been received more and more attentions, see, e.g., Refs. [13–17] and references therein. However, among these works, a simple double-well form of free-energy density is usually used, which is inaccurate to simulate realistic hydrocarbon species in a binary fluid systems. Recently, there have been several efforts devoted to diffuse interface models with realistic Peng-Robinson (P-R) equation of state (EOS). In Ref. [18], a diffuse interface model with P-R EOS was developed. By using this model, the qualitative behavior of multiphase hydrocarbon systems can be resolved. Whereafter, a semi-implicit energy stable time marching scheme with a mixed finite element space discretization was designed to solve this model. A realistic hydrocarbon system with isobutane in two spatial

dimension has been simulated in this work. Fan *et al.* [19] extended the above work to multicomponents two-phase fluids systems with Van der Waals and P-R equation of states. A component-wise convex splitting semi-implicit scheme was proposed to solve the multicomponent hydrocarbon systems. In their numerical examples, a mixture consists of methane and *n*-decane on a two dimensional disk domain has been simulated. Hereafter, aimed at the fourth-order parabolic equation in the diffuse interface model with P-R EOS, Peng *et al.* [20,21] used convex-splitting scheme and second order energy stable scheme to solve it, respectively. Furthermore, based on the recently developed invariant energy quadratization (IEQ) approach [22], Li *et al.* [23] designed first and second order schemes for temporal discretization of the diffuse interface model with P-REOS. Aforementioned works were focus on the static behavior of two-phase fluid systems. In the work of Kou and Sun [24], multicomponent two-phase flow problems with partial miscibility based on P-R EOS were numerically studied by a multiscale numerical method. Several two-dimensional droplet deformation problems were simulated to verify the effectiveness of the proposed multiscale method. From the above, we can see that a variety of numerical schemes have been designed to solve the diffuse interface model with P-R EOS. However, the phase equation derived from P-R free-energy model involves high nonlinearity, which brings great challenges to design numerical schemes. And also based on the fact that the transport process of hydrocarbon fluids in subsurface is very complicated, it is highly desired to develop effective and easy-to-implement numerical schemes for three dimensional multiphase fluid systems with realistic EOS.

In recent years, the lattice Boltzmann method (LBM), which is originated from lattice gas automata (LGA) and also could be derived from the kinetic Boltzmann equation, has emerged as an alternative powerful method for simulating complex fluid dynamics problems [25–27]. The kinetic nature brings many advantages to the LBM, including clear physical pictures,

*xuguangcscs@hust.edu.cn

simple algorithm structure, easy implementation of boundary conditions and natural parallelism. In addition, it is also very easy to incorporate internal interactions between the fluid and external environment at the mesoscopic level, which makes the LBM very suitable for simulating multicomponent and multiphase flows. Up to now, various types of lattice Boltzmann methods (LBMs) for multiphase and multicomponent flows have been constructed from different viewpoints, such as the color-fluid model [28], the pseudopotential model [29,30], the free-energy model [31,32], the kinetic model based on Enskog equation [33,34], and the phase field model (or diffuse interface model or mean field theory model) [35–38]. Among these, due to aforementioned attractive features, the phase-field based LBM has become a popular and widely used method for simulating multiphase flows with low and large density ratios. Several improved LB models for the Navier-Stokes-Cahn-Hilliard coupled system were also developed [39–44]. These marvelous multiphase LBMs have achieved remarkable success in simulating various interfacial flows. However, most of above-mentioned phase-field-based LBMs are developed based on the double-well form of free-energy density, which is hardly to simulate the multiphase system quantitatively. Very recently, the entropic lattice Boltzmann method (ELBM) [45–47] has been extended to simulate realistic multiphase flows [48], where the entropy is introduced at each lattice and increased for each time step. In this work, a modified P-R EOS, with proven superior stability and performance for dynamic simulations, is introduced. In the work by Mazloomi [49,50] and Bösch *et al.* [51], the ELBM-based free-energy multiphase model has been successfully applied to simulate droplet dynamics. In addition, in the work by Qin *et al.* [52], through coupling the entropic multiple-relaxation-time (EMRT) LBM with a multirange pseudopotential model, the complex fluid flow for a wide range of kinematic viscosity and surface tension at a high density ratio in two- and three-dimensional applications can be simulated.

In this work, to simulate realistic hydrocarbon species in a binary fluid systems accurately, we will develop a mass conservative LB scheme for three dimensional diffuse interface model with P-R EOS. Phase separations at different temperatures in 3D space of two hydrocarbon species, including nC_4 and C_3 , will be simulated by using the proposed mass conservative LBM. The computed interface tension will be compared with laboratory data. The rest of this paper is organized as follows. In Sec. II, we will present the general mathematical model for multicomponent binary fluid systems based on a realistic EOS, in which the Allen-Cahn-type phase equation with a Lagrange multiplier is derived. In Sec. III, the mass conservative LB scheme for this equation is developed and the definition of the Lagrange multiplier is also discussed based on the framework of LB scheme. Several 3D numerical examples, including realistic species of isobutane and propane, are simulated in Sec. IV. Finally, some conclusions are given in Sec. V.

II. DIFFUSE INTERFACE MODEL FOR MULTIPHASE FLUID SYSTEMS

A. Thermodynamic relations revisit

The fluid mixture consisting of a fixed number of species with a constant temperature T is considered in this study.

We denote the number of components in the fluid mixture by M , the molar density vector is denoted by \mathbf{n} with the expression of

$$\mathbf{n} = (n_1, n_2, \dots, n_M)^T = \frac{(N_1, N_2, \dots, N_M)^T}{V}, \quad (1)$$

where n_i represents the molar density of the component i , N_i is the mole of i th component, V is the overall volume, and $n = n_1 + n_2 + \dots + n_M$ is the molar density of the fluid.

From fundamental law of thermodynamics, we have the following equation:

$$U = TS - pV + \sum_{i=1}^M \mu_i N_i, \quad (2)$$

where U is the internal energy, T is the temperature, S is the entropy, p is the pressure, and μ_i is the chemical potential of component i .

The Helmholtz free energy has the form $F = U - TS$. Based on it, we define Helmholtz free-energy density as $f = F/V$, and then we can get

$$f = -p + \sum_{i=1}^M \mu_i n_i. \quad (3)$$

Since we consider a constant temperature system, the following formula can be obtained by the Gibbs-Duhem equation,

$$dp = \sum_{i=1}^M n_i d\mu_i, \quad (4)$$

and then, substituting Eq. (4) into Eq. (3), one can get

$$df = \sum_{i=1}^M \mu_i dn_i. \quad (5)$$

From the above thermodynamic relations, we can see that f is a function of \mathbf{n} under a constant temperature. Once $f(\mathbf{n})$ is given, the chemical potential μ_i and pressure p can be computed as

$$\mu_i = \left(\frac{\delta f(\mathbf{n})}{\delta n_i} \right)_{\mathbf{n}_{\neq i}}, \quad i = 1, \dots, M, \quad (6)$$

$$p = \sum_{i=1}^M \mu_i n_i - f(\mathbf{n}), \quad (7)$$

where $\delta/\delta n_i$ represents the variational derivative and $\mathbf{n}_{\neq i}$ is denoted by the vector

$$(n_1, \dots, n_{i-1}, n_{i+1}, \dots, n_M).$$

B. Formation of the Helmholtz free energy with P-R EOS

In the realistic inhomogeneous fluid system, the diffuse interfaces always exist between different phases. To describe this phenomenon, the local density gradient contribution is introduced into the Helmholtz free-energy density f . Then f can be expressed as the sum of two contributions, one is the Helmholtz free-energy density of bulk homogeneous fluid (denoted by f_0) and the other is the contribution of the local

density gradient (denoted by f_{∇}):

$$f(\mathbf{n}) = f_0(\mathbf{n}) + f_{\nabla}(\mathbf{n}). \quad (8)$$

The definition of $f_0(\mathbf{n})$ is based on the selected EOS. In this work, the realistic P-R EOS [53], which is widely used in the oil industries and petroleum engineering, is considered. Then, $f_0(\mathbf{n})$ is expressed as summation of two terms, ideal part and excess one [18,19],

$$f_0(\mathbf{n}) = f_0^{\text{ideal}}(\mathbf{n}) + f_0^{\text{excess}}(\mathbf{n}), \quad (9)$$

$$f_0^{\text{ideal}}(\mathbf{n}) = RT \sum_{i=1}^M n_i (\ln n_i - 1), \quad (10)$$

$$f_0^{\text{excess}}(\mathbf{n}) = -nRT \ln(1 - bn) + \frac{an}{2\sqrt{2}b} \ln \left(\frac{1 + (1 - \sqrt{2})bn}{1 + (1 + \sqrt{2})bn} \right), \quad (11)$$

where R denotes the universal gas constant with the value of $8.31432 \text{ JK}^{-1} \text{ mol}^{-1}$. The parameters $a = a(T)$ and b are the energy parameter and the covolume parameter, respectively. The definition of these two parameters can be found in the Appendix.

The gradient free energy $f_{\nabla}(\mathbf{n})$ is described by a simple quadratic relation,

$$f_{\nabla}(\mathbf{n}) = \frac{1}{2} \sum_{i,j=1}^M c_{ij} \nabla n_i \cdot \nabla n_j, \quad (12)$$

where c_{ij} is the cross influence parameter, which is given in the Appendix.

The pressure of homogeneous fluids p_0 is related to the Helmholtz free energy $f_0(\mathbf{n})$ in the following way:

$$p_0 = p_0(\mathbf{n}, T) = \sum_{i=1}^M n_i \left(\frac{\partial f_0}{\partial n_i} \right) - f_0 = \sum_{i=1}^M n_i \mu_{0,i} - f_0. \quad (13)$$

Replacing f_0 and $\mu_{0,i}$, we have the following P-R EOS:

$$p_0 = \frac{nRT}{1 - bn} - \frac{n^2 a(T)}{1 + 2bn - b^2 n^2}. \quad (14)$$

In addition, from the free-energy density of P-R EOS, the total chemical potential consists of two contributions, one from homogeneous fluid theory and the other from the gradient theory, which can be computed by

$$\mu_i = \left(\frac{\delta f(\mathbf{n})}{\delta n_i} \right)_{\mathbf{n}_{\neq i}} = \mu_{0,i}(\mathbf{n}) - \sum_{j=1}^M \nabla \cdot (c_{ij} \nabla n_j), \quad (15)$$

$$i = 1, 2, \dots, M,$$

where $\mu_{0,i} = (\partial f_0(\mathbf{n}) / \partial n_i)_{\mathbf{n}_{\neq i}}$.

C. Derivation of the Allen-Cahn-type phase equation

In this work, following the same assumption in Ref. [18], we present the Allen-Cahn-type equation for the single-

component two-phase system as follows:

$$\frac{\partial n(\mathbf{x}, t)}{\partial t} - \kappa \nabla^2 n(\mathbf{x}, t) = \zeta(t) - \mu_0(\mathbf{x}, t), \quad \mathbf{x} \in \Omega, \quad (16)$$

$$\int_{\Omega} n(\mathbf{x}, t) d\mathbf{x} = N, \quad (17)$$

where κ is the influence parameter, and $\zeta(t)$ is the Lagrange multiplier to enforce the mass conservation. From the homogeneous free-energy density of P-R EOS, the homogeneous chemical potential μ_0 can be expressed as the following nonlinear form:

$$\mu_0 = RT \ln \frac{n}{1 - bn} + RT \frac{bn}{1 - bn} + \frac{a}{2\sqrt{2}b} \times \ln \left(\frac{1 + (1 - \sqrt{2})bn}{1 + (1 + \sqrt{2})bn} \right) - \frac{an}{1 + bn + bn(1 - bn)}. \quad (18)$$

Through selecting proper initial conditions and boundary conditions, together with a specified bulk chemical potential μ_0 , the above system has a unique solution [18].

The strong nonlinearity in the source term of Eq. (16) and the quite small values of κ give rise to a great challenge of the numerical simulation. In the following section, we will develop an efficient LB method for the above nonlinear A-C type phase equation, and the definition of $\zeta(t)$ will also be discussed in detail. Our method can be extended to the multicomponent case, as in Ref. [19].

III. LB METHOD FOR THE A-C-TYPE PHASE EQUATION WITH P-R EOS

In fact, the LB method can be viewed as a special finite difference (FD) scheme for the following continuous Boltzmann equations with discrete velocity space \mathbf{e}_i ($i = 1, 2, \dots, N$) [27]:

$$\frac{\partial g_i(\mathbf{x}, t)}{\partial t} + \mathbf{c}_i \cdot \nabla g_i(\mathbf{x}, t) = -\frac{1}{\tau_0} [g_i(\mathbf{x}, t) - g_i^{\text{eq}}(\mathbf{x}, t)], \quad (19)$$

where N is the number of different velocities in this model, $g_i(\mathbf{x}, t)$ is the discrete distribution function at site \mathbf{x} and time t moving with speed c along the direction \mathbf{e}_i and $\mathbf{c}_i = c\mathbf{e}_i$. $g_i^{\text{eq}}(\mathbf{x}, t)$ is the local equilibrium distribution function depending on the macroscopic variables, and τ_0 represents the relaxation time toward the equilibrium distribution. This model reflects that the distribution function relaxes to the equilibrium state with collisions.

If we use the first-order forward difference scheme to discretize the time derivative term, use the up-wind scheme for the spatial gradient term, and use a downwind collision term, we can get the following FD scheme for Eq. (19):

$$g_i(\mathbf{x}, t + \delta t) = g_i(\mathbf{x}, t) - \alpha [g_i(\mathbf{x}, t) - g_i(\mathbf{x} - \mathbf{D}_i, t)] - \frac{1}{\tau} [g_i(\mathbf{x} - \mathbf{D}_i, t) - g_i^{\text{eq}}(\mathbf{x} - \mathbf{D}_i, t)], \quad (20)$$

where \mathbf{D}_i is the spatial displacement of the i th discrete velocity, $\alpha = \delta t |\mathbf{c}_i| / |\mathbf{D}_i|$, and $\tau = \tau_0 / \delta t$ is the dimensionless relaxation

time. If $\alpha = 1$, i.e., $\mathbf{D}_i = \mathbf{c}_i \delta t$, the following standard LB equation can be obtained:

$$g_i(\mathbf{x} + \mathbf{c}_i \delta t, t + \delta t) = g_i(\mathbf{x}, t) - \frac{1}{\tau} [g_i(\mathbf{x}, t) - g_i^{\text{eq}}(\mathbf{x}, t)]. \quad (21)$$

The key element in applying LBM for different problems is the equilibrium distribution function. The general form of the equilibrium distribution function can be written as [54]

$$g_i^{\text{eq}} = \omega_i \left\{ \phi + \frac{\mathbf{c}_i \cdot \mathbf{B}}{c_s^2} + \frac{[\mathbf{C} + c_s^2(\mathbf{D} - \phi \mathbf{I})] : (\mathbf{c}_i \mathbf{c}_i - c_s^2 \mathbf{I})}{2c_s^4} \right\}, \quad (22)$$

where \mathbf{I} is the unit tensor, ϕ stands for scalar parameter, such as density ρ , temperature, or species concentration, \mathbf{B} and \mathbf{D} are differential functions of ϕ , and \mathbf{C} is a tensor function of ϕ , which is used to remove some additional terms in the recovered macroscopic equation. Besides, ω_i are weights and c_s is the so-called sound speed, being related to the particle speed c and ω_i by $\sum_i \omega_i \mathbf{c}_i \mathbf{c}_i = c_s^2 \mathbf{I}$, and they all depend on the lattice model used, where $c = \delta x / \delta t$ and δx is the lattice spacing.

By means of the multiscale Chapman-Enskog analysis [54], the above LB method can recover the following convection-diffusion equation:

$$\partial_t \phi + \nabla \cdot \mathbf{B} = \nabla \cdot (\alpha \nabla \cdot \mathbf{D}), \quad (23)$$

where α is the diffusion coefficient.

Following the above idea, we can get the LB method for Eq. (16) as follows:

$$g_i(\mathbf{x} + \mathbf{c}_i \delta t, t + \delta t) = g_i(\mathbf{x}, t) - \frac{1}{\tau} [g_i(\mathbf{x}, t) - g_i^{\text{eq}}(\mathbf{x}, t)] + \delta t R_i(\mathbf{x}, t), \quad (24)$$

where the local equilibrium distribution function $g_i^{\text{eq}}(\mathbf{x}, t)$ and the distribution function for source term $R_i(\mathbf{x}, t)$ are defined as

$$g_i^{\text{eq}}(\mathbf{x}, t) = \omega_i n(\mathbf{x}, t),$$

$$R_i(\mathbf{x}, t) = \omega_i [\zeta(t) - \mu_0(\mathbf{x}, t)].$$

By the definition of the above distribution functions, moment conditions can be computed explicitly providing the following lattice symmetries:

$$\begin{aligned} \sum_{i=1}^N \omega_i &= 1, & \sum_{i=1}^N \omega_i \mathbf{c}_i \mathbf{c}_i &= c_s^2 \mathbf{I} = c_s^2 \delta_{ij}, \\ \sum_{i=1}^N \omega_i \mathbf{c}_i &= \mathbf{0}, & \sum_{i=1}^N \omega_i \mathbf{c}_i \mathbf{c}_i \mathbf{c}_i &= \mathbf{0}, & \sum_{i=1}^N \omega_i \mathbf{c}_i \mathbf{c}_i \mathbf{c}_i \mathbf{c}_i &= \mathbf{0}, \\ \sum_{i=1}^N \omega_i \mathbf{c}_i \mathbf{c}_i \mathbf{c}_i \mathbf{c}_i &= c_s^4 \Delta = c_s^4 (\delta_{ij} \delta_{kl} + \delta_{ik} \delta_{jl} + \delta_{il} \delta_{jk}). \end{aligned} \quad (25)$$

 TABLE I. Parameters of some $DnQm$ models.

Model	Lattice vector \mathbf{e}_i	Weight ω_i	c_s^2
D1Q3	$0, \pm 1$	$2/3, 1/6$	$1/3$
D2Q9	$(0, 0), (\pm 1, 0), (0, \pm 1), (\pm 1, \pm 1)$ $(0, 0, 0)$	$4/9, 1/9, 1/36$ $1/3$	$1/3$
D3Q15	$(\pm 1, 0, 0), (0, \pm 1, 0), (0, 0, \pm 1)$ $(\pm 1, \pm 1, 0), (\pm 1, 0, \pm 1), (0, \pm 1, \pm 1)$	$1/18$ $1/36$	$1/3$

Therefore, the following moment conditions can be derived:

$$\begin{aligned} \sum_{i=1}^N g_i^{\text{eq}}(\mathbf{x}, t) &= \sum g_i(\mathbf{x}, t) = n(\mathbf{x}, t), \\ \sum_{i=1}^N \mathbf{c}_i g_i^{\text{eq}}(\mathbf{x}, t) &= \mathbf{0}, & \sum_{i=1}^N \mathbf{c}_i \mathbf{c}_i g_i^{\text{eq}}(\mathbf{x}, t) &= c_s^2 n(\mathbf{x}, t) \mathbf{I}, \\ \sum_{i=1}^N R_i(\mathbf{x}, t) &= \zeta(t) - \mu_0(\mathbf{x}, t), & \sum_{i=1}^N \mathbf{c}_i R_i(\mathbf{x}, t) &= \mathbf{0}, \\ \sum_{i=1}^N \mathbf{c}_i \mathbf{c}_i R_i(\mathbf{x}, t) &= c_s^2 [\zeta(t) - \mu_0(\mathbf{x}, t)] \mathbf{I}. \end{aligned} \quad (26)$$

In general, the $DnQm$ lattice model (n dimensional m velocity), which is proposed by Qian *et al* [55], is widely used in the LB method. In Table I, several popular $DnQm$ models are presented.

A. Chapman-Enskog analysis of the present LB method

The basic idea of Chapman-Enskog expansion is to separate the physical time and space as well as distribution function into multiple scales with respect to a small parameter ε (its value is proportional to Knudsen number Kn). Physical properties of the macroscopic variables are automatically separated into the corresponding different scales.

The distribution function can be expanded in terms of ε as

$$g_i = g_i^{(0)} + \varepsilon g_i^{(1)} + \varepsilon^2 g_i^{(2)} + \dots, \quad (27)$$

where $g_i^{(0)}$ is distribution function at the equilibrium conditions, equal to g_i^{eq} . By summing the above equation with respect to i ,

$$\sum_{i=1}^N g_i = \sum_{i=1}^N [g_i^{(0)} + \varepsilon g_i^{(1)} + \varepsilon^2 g_i^{(2)} + \dots]. \quad (28)$$

From Eq. (26), the other expanded term in the above equation should be zero, i.e.,

$$\sum_{i=1}^N g_i^{(k)} = 0, \quad k \geq 1. \quad (29)$$

Generally, the time t and space \mathbf{x} are scaled in the following way:

$$\mathbf{x} = \varepsilon^{-1} \mathbf{x}_1, \quad t_1 = \varepsilon t, \quad t_2 = \varepsilon^2 t. \quad (30)$$

In this representation, \mathbf{x}_1, t_1 describe the linear regime, or the fast convective scale, whereas t_2 is in charge of the long term

dynamics, or slow diffusive scale. Notice that Eq. (16) is a diffusion equation with source term, to keep both sides of the equation at the same order of magnitude, the time t should be scaled by $1/\varepsilon^2$, i.e., $t = \varepsilon^{-2}t_2$. Thus, the source term $\zeta - \mu_0$ can be expanded as follows:

$$\zeta - \mu_0 = \varepsilon^2(\zeta - \mu_0)^{(2)}. \quad (31)$$

The above multiscale representation induces a corresponding representation of the differential operators:

$$\frac{\partial}{\partial t} = \varepsilon^2 \frac{\partial}{\partial t_2}, \quad \nabla = \varepsilon \nabla_1. \quad (32)$$

Using the above multiscale Chapman-Enskog expansions, by applying Taylor expansion to the evolution Eq. (24), and analyze it in different scales, we can get the following equations:

$$O(\varepsilon): \quad \mathbf{c}_i \cdot \nabla_1 g_i^{\text{eq}} = -\frac{1}{\tau \delta t} g_i^{(1)}, \quad (33)$$

$$O(\varepsilon^2): \quad \partial_{t_2} g_i^{\text{eq}} + \left(1 - \frac{1}{2\tau}\right) \mathbf{c}_i \cdot \nabla_1 g_i^{(1)} = -\frac{1}{\tau \delta t} g_i^{(2)} + R_i^{(2)}, \quad (34)$$

where $R_i^{(2)} = \omega_i(\zeta - \mu_0)^{(2)}$.

With the aid of Eq. (26), Eqs. (33) and (34) can be integrated as

$$O(\varepsilon^2): \quad \partial_{t_2} n + \left(1 - \frac{1}{2\tau}\right) \nabla_1 \cdot \sum_i \mathbf{c}_i g_i^{(1)} = (\zeta - \mu_0)^{(2)}. \quad (35)$$

Using Eqs. (26) and (33), we can get

$$\sum_i \mathbf{c}_i g_i^{(1)} = -\tau \delta t \nabla_1 \cdot \sum_i \mathbf{c}_i \mathbf{c}_i g_i^{\text{eq}} = -\tau \delta t (\nabla_1 \cdot c_s^2 n \mathbf{I}). \quad (36)$$

And then, substituting Eq. (36) into Eq. (35) and combining the equation on ε^2 scale, the following equation can be recovered:

$$\frac{\partial n(\mathbf{x}, t)}{\partial t} = \kappa \nabla^2 n(\mathbf{x}, t) + \zeta(t) - \mu_0(n(\mathbf{x}, t)),$$

where we enforce $c_s^2(\tau - 1/2)\delta t = \kappa$.

B. The definition of Lagrange multiplier

To guarantee the mass conservation of the proposed LB scheme, the Lagrange multiplier $\zeta(t)$ must be defined in a right way. To explore the relationship between $\zeta(t)$ and the proposed LB scheme, we expand Eq. (24) at $(x, y, z) \in \Omega$ and time $t + \delta t$ under the most used D3Q15 model as follows:

$$\begin{aligned} g_0(x, y, z, t + \delta t) &= \left(1 - \frac{1}{\tau}\right) g_0(x, y, z, t) + \frac{1}{\tau} \omega_0 n(x, y, z, t) + \delta t \omega_0 [\zeta(t) - \mu_0(x, y, z, t)], \\ g_1(x, y, z, t + \delta t) &= \left(1 - \frac{1}{\tau}\right) g_1(x - \delta x, y, z, t) + \frac{1}{\tau} \omega_1 n(x - \delta x, y, z, t) + \delta t \omega_1 [\zeta(t) - \mu_0(x - \delta x, y, z, t)], \\ &\dots \\ g_{14}(x, y, z, t + \delta t) &= \left(1 - \frac{1}{\tau}\right) g_{14}(x - \delta x, y + \delta y, z + \delta z, t) + \frac{1}{\tau} \omega_{14} n(x - \delta x, y + \delta y, z + \delta z, t) \\ &\quad + \delta t \omega_{14} [\zeta(t) - \mu_0(x - \delta x, y + \delta y, z + \delta z, t)]. \end{aligned} \quad (37)$$

From the above expansions, if we sum all the nodes in Ω , the following equation can be obtained:

$$\begin{aligned} \sum_{x,y,z=0}^M n(x, y, z, t + \delta t) &= \sum_{x,y,z=0}^M n(x, y, z, t) \\ &\quad + \delta t \sum_{x,y,z=0}^M [\zeta(t) - \mu_0(x, y, z, t)], \end{aligned} \quad (38)$$

where M is the grid number. To satisfy the mass conservation, $\zeta(t)$ must be defined in the following way:

$$\zeta(t) = \frac{1}{(M+1)^3} \sum_{x,y,z=0}^M \mu_0(x, y, z, t). \quad (39)$$

It is worth mentioning that the above derivation is based on the periodic boundary condition. However, it can also be applied to the standard bounce-back boundary condition.

IV. NUMERICAL EXPERIMENTS

In this section, several numerical experiments, including the test of thermodynamic consistency with coexistence curves, the simulation of realistic hydrocarbon species, and the validation of Young-Laplace equation, are carried out to verify the effectiveness of the presented LB method.

A. The two-phase coexistence densities

The two-phase coexistence densities solved by the Maxwell equal-area construction are used as the benchmark to verify the thermodynamic consistency of the presented LB method. In this work, the P-R EOS, which is widely used in the oil industries and petroleum engineering, is investigated. With horizontal phase interfaces, the middle part of the domain is initialized as liquid, and the remaining part is set as gas. The computational domain is a 127×127 square with periodical boundary condition. The value of κ is set to be 0.01. The reduced variables $T_r = T/T_c$ and $\rho_r = \rho/\rho_c$, where T_c and ρ_c are the critical temperature and the critical density, respectively. The parameters are set as $a(T) = \frac{2}{49}[1 + (0.37464 + 1.54226\omega - 0.26992\omega^2) \times (1 - \sqrt{T/T_c})]^2$, with

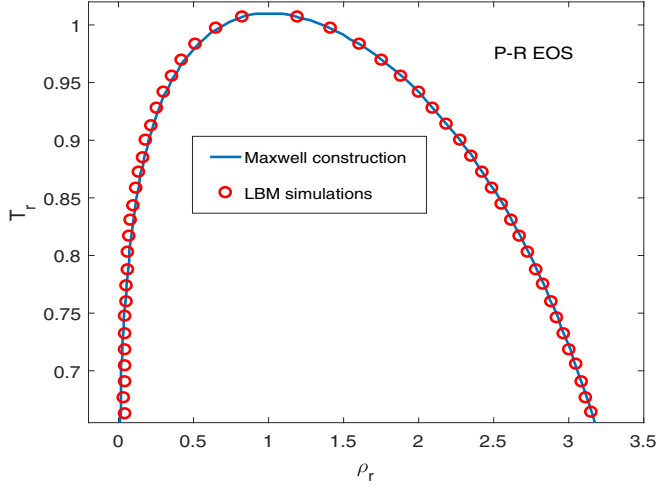


FIG. 1. Two-phase coexistence curve.

the acentric factor $\omega = 0.344$, $b = 2/21$, and $R = 1$. Thus, the critical temperature and density are $T_c = 0.072919$ and $\rho_c = 2.657304$, respectively. As shown in Fig. 1, the resulted coexistence densities of P-R EOS agree well with the benchmark solutions by Maxwell equal-area construction. These results numerically confirm that the present LB method is thermodynamically consistent.

B. Numerical simulations of realistic hydrocarbon species

In this subsection, we will consider the two-phase separation of isobutane (nC_4) and propane (C_3) separately at different temperatures, where the D3Q15 lattice model will be used. In the numerical simulations, to simplify the computational process, the original domain $\Omega = (0, L)^3$, where $L = 2 \times 10^{-8}$ meters, is projected to its normalized map $\hat{\Omega} = [0, \hat{L}]^3$, where $\hat{L} = L \times 10^8$. The whole discrete domain Ω has $200 \times 200 \times 200$ uniform cube grids. The time step $\delta t = \delta x/c$, and $1 \leq c \leq 2$ is related to lattice sound speed. The critical properties and the normal boiling point of nC_4 and C_3 are given in Table II. Thus, following the definition of P-R parameters a , b and the acentric factor ω , which can be found in Ref. [1], the values of these parameters can be calculated. The detailed values of the influence parameter κ , a and the initial values of nC_4 and C_3 at different temperatures are provided in Tables III and IV, respectively.

In simulations, the initial condition is to impose the liquid density of hydrocarbons (n_l) under saturated pressure condition at 333.28 K in the region of $(0.3L, 0.7L)^3$, and the rest of the domain is filled with saturate gas of hydrocarbons (n_g) under the same temperature. The periodic boundary condition is imposed as in Refs. [20,21]. The spatial distributions of

 TABLE II. Relevant data of nC_4 and C_3 .

Symbol	T_c (K)	P_c (MPa)	T_b (K)	ω	b
nC_4	425.18	3.797	272.64	0.2055	7.2433×10^{-5}
C_3	369.82	4.250	231.05	0.1579	5.6287×10^{-5}

 TABLE III. Values of κ , a , and initial molar densities of nC_4 .

T	a	κ	n_g	n_l
255.02K	2.0020	1.9285×10^{-3}	22.082	1.1274×10^4
270.90K	1.9463	1.9582×10^{-3}	43.757	1.0939×10^4
285.43K	1.8974	1.9834×10^{-3}	71.480	1.0639×10^4
299.48K	1.8519	2.0060×10^{-3}	109.81	1.0321×10^4
315.82K	1.8010	2.0302×10^{-3}	173.08	0.9912×10^4
333.28 K	1.7487	2.0536×10^{-3}	270.37	0.9419×10^4

molar densities for nC_4 at different moments have been depicted in Fig. 2. Initially, a cubic droplet is given, after 200 time steps, we can see in Fig. 2(a) that the shape of the droplet is still in cube-shape. After 500 time steps, four corners of the droplet being rounded [see Fig. 2(b)]. At last, the droplet shape appears to be a perfect sphere in Fig. 2(c).

Furthermore, the coalescence of the separated droplets consisting of C_3 at at $T = 329.79$ K is also numerically simulated. Different from the simulation of nC_4 , four separated cubic droplets are given as the initial state. When the gaps between the droplets are less than twice of the interface thickness, the merging of the separated droplets will occur due to surface tension. Figure 3 shows the evolution of the interfacial shapes of the separated droplets merged under capillary force. The quantitative comparison with laboratory data will be listed in the next section.

In the diffuse interface model, the homogeneous chemical potential density μ_0 , the surface tension contributed to the Helmholtz free-energy density f_{intfTens} and the thermodynamic pressure p_0 at the steady state are the most concerned variables. Among them, μ_0 and p_0 are defined in Eqs. (13) and (14), and f_{intfTens} has the same expression as that presented in the work by Qiao and Sun [18],

$$f_{\text{intfTens}} = 2f_{\nabla}(n) = \kappa \nabla n \cdot \nabla n. \quad (40)$$

The following relationship can be given:

$$\begin{aligned} F(n) - F_0(n_{\text{init}}) &= \int_{\Omega} [f_0(n) - f_0(n_{\text{init}})] dx + \int_{\Omega} f_{\nabla}(n) dx \\ &\cong \int_{\Omega} f_{\text{intfTens}} dx. \end{aligned} \quad (41)$$

Without loss of generality, we will take nC_4 as an example. Numerical results of the above variables after convergence are depicted in Fig. 4. It can be found that all these variables experience a sharp variation at the interface at the steady state. In particular, the homogeneous contribution of chemical

 TABLE IV. Values of κ , a , and initial molar densities of C_3 .

T	a	κ	n_g	n_l
253.08K	1.2434	1.1926×10^{-3}	1.2357×10^2	1.3412×10^4
267.09K	1.2125	1.2095×10^{-3}	1.9407×10^2	1.2921×10^4
279.39K	1.1864	1.2235×10^{-3}	2.7939×10^2	1.2445×10^4
295.73K	1.1530	1.2406×10^{-3}	4.3805×10^2	1.1732×10^4
315.71K	1.1140	1.2596×10^{-3}	7.3396×10^2	1.0697×10^4
329.79K	1.0876	1.2717×10^{-3}	1.1462×10^3	9.5705×10^3

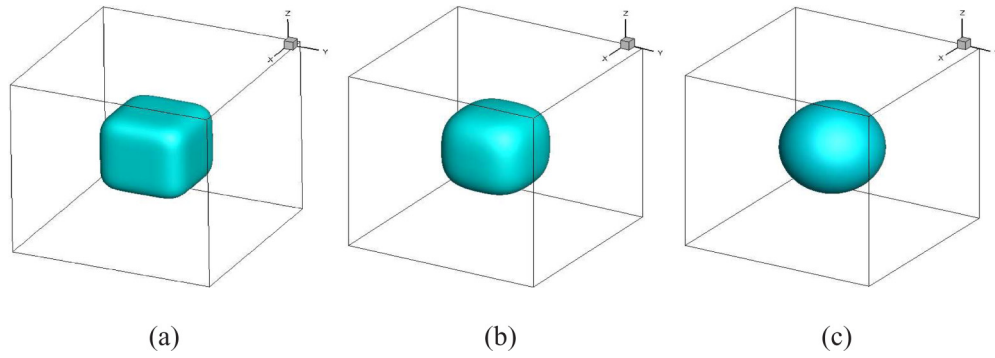


FIG. 2. Numerical results of nC_4 at different time points: (a) $t = 200$, (b) $t = 500$, (c) $t = 1000$.

potential μ_0 changes dramatically across the interface even though it must have the same value in the liquid and gas bulk regions.

To illustrate the energy stability of the corresponding LB method, the time varying total Helmholtz free energy is depicted in Fig. 5(a). It can be clearly seen that the free energy has a dissipative trend during the whole evolution history, and it decays rapidly initially and slows down in the rest of time.

This illustrates that the solution approaches its steady state. In addition, from Fig. 5(b), we can see that the mass conservation property has been maintained strictly.

In addition, spurious current emerging in the vicinity of phase interface is a well-known undesirable feature of the LBM for two-phase flows. In this study, to observe how the velocity field is altered by the spurious currents, the velocity field of the nC_4 droplet at $T = 333.28$ K in two dimensions

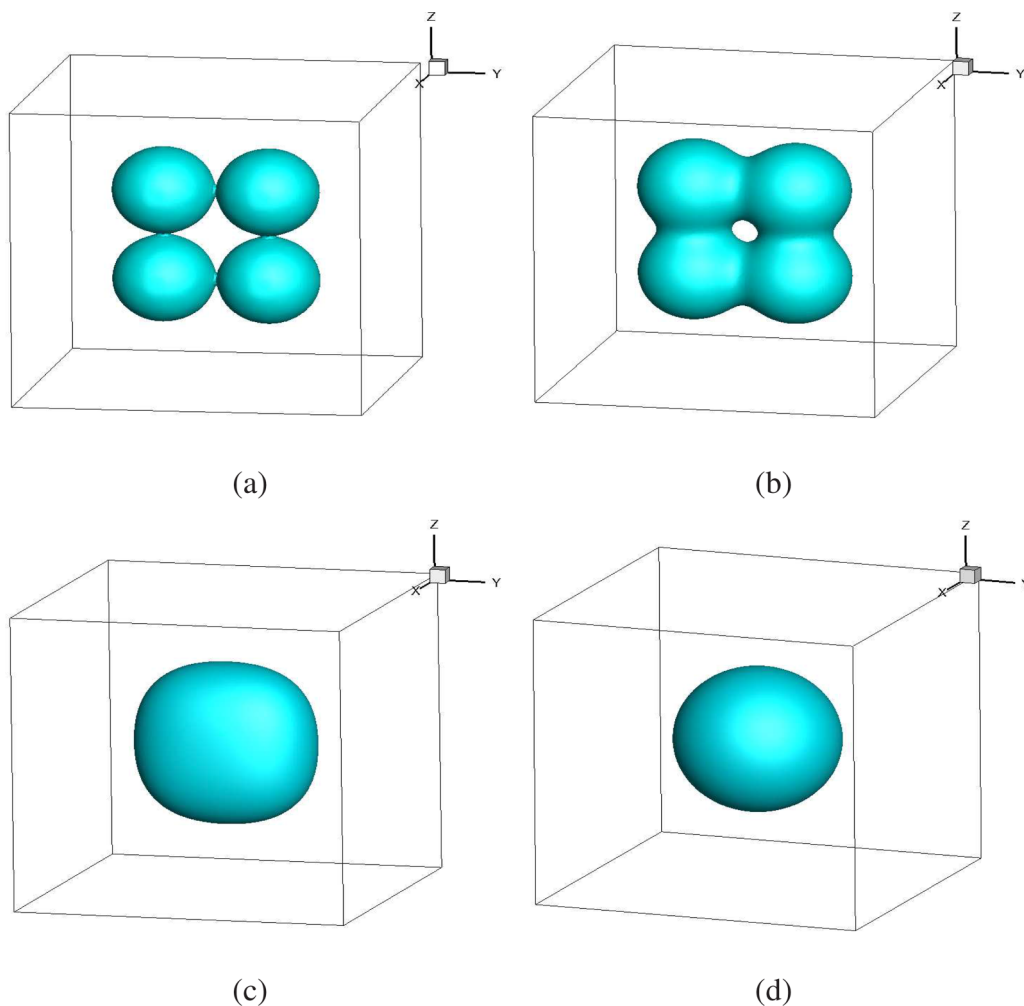


FIG. 3. Numerical results of C_3 at different time points: (a) $t = 100$, (b) $t = 500$, (c) $t = 1500$, (d) $t = 4000$.

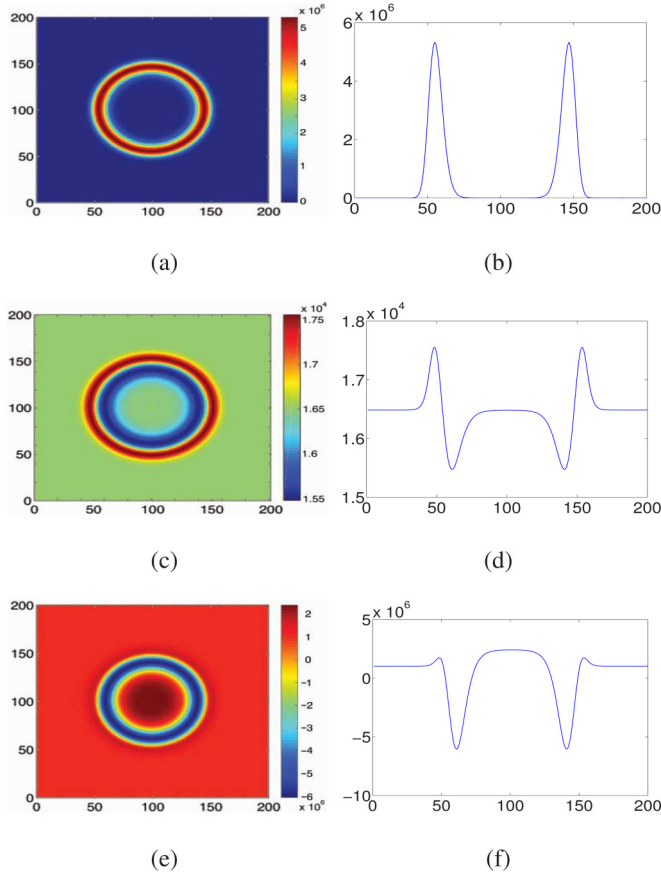


FIG. 4. 3D profile along $Z = L/2$ after convergence (nC_4 at $T=333.28$ K): (a) surface tension contribution of Helmholtz free-energy density, (b) cross profile of (a); (c) homogeneous contribution of chemical potential, (d) cross profile of (c); (e) thermal pressure, (f) cross profile of (e).

is shown in Fig. 6(a). It can be seen that eight eddies are formed near the droplet interface. The magnitude of the spurious currents is evaluated by the average kinetic energy $E = \int \frac{1}{2} |\mathbf{u}|^2 d\mathbf{x}$. As seen from the time histories of the average

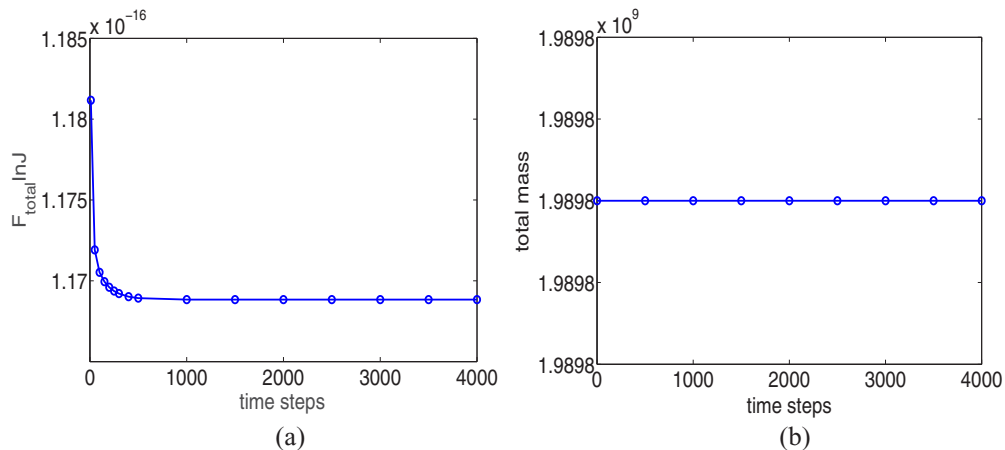


FIG. 5. Energy dissipation and mass conservation of 3D numerical simulation of nC_4 : (a) energy dissipation, (b) total mass variation with time.

kinetic energy shown in Fig. 6(b), the magnitude of the spurious currents decreases as time evolves and reaches a steady-state value.

C. Calculation of interface tension

To verify our numerical results of nC_4 and C_3 quantitatively, the interface tension σ has been computed and compared with previous numerical results and laboratory data.

Traditionally, the surface tension is defined as the net contractive force per unit length of interface with a unit of N/m or the work for creating a unit area of interface with a unit of J/m^2 :

$$\sigma = \frac{F(n) - F_0(n_{\text{init}})}{A} \cong \frac{\int_{\Omega} f_{\text{intfTens}} d\mathbf{x}}{A}, \quad (42)$$

with the assumption that σ is spatially constant within the interface for the given system and A is the surface area of the droplet.

In the previous work by Qiao and Sun [18], which considers the problem in two dimension, the radius of the droplet is determined based on the assumption that the area of the droplet does not change with time, which has the following form

$$r_{2D} = \left(\frac{1}{\pi} A \right)^{\frac{1}{2}}. \quad (43)$$

Similarly, in the work by Li *et al.* [23], which considers the problem in three dimensions, the radius is calculated under the same assumption. The radius in their work has the form

$$r_{3D} = \left(\frac{3}{4\pi} V \right)^{\frac{1}{3}}, \quad (44)$$

where V is the volume of the droplet. It should be noted that these assumptions are developed from the sharp interface theory, which are unsuitable for simulations based on the diffuse interface theory [18,23]. Hence, the width of the two-phase interface should be considered while calculating the radius of the droplet. Following the definition of interfacial

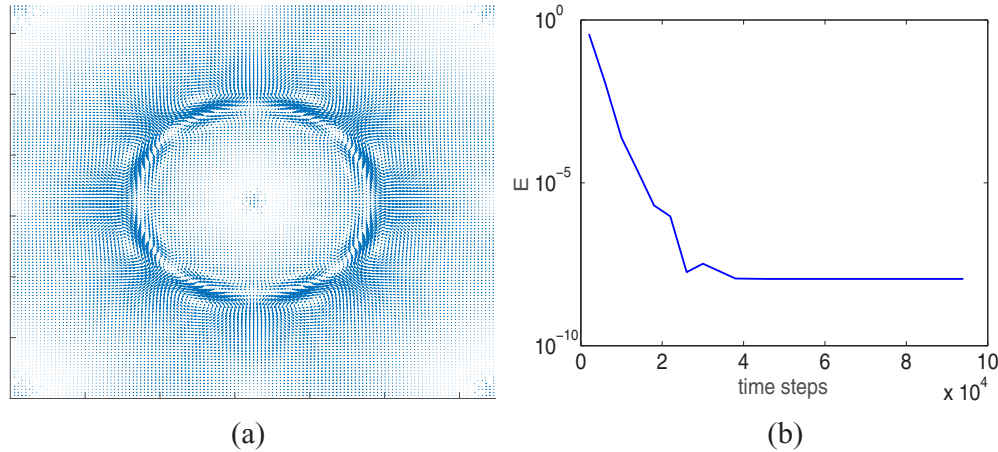


FIG. 6. (a) velocity field of the nC_4 droplet at $T=333.28$ K, (b) time history of the average kinetic energy.

thickness in Ref. [56], the estimation of the width of the diffuse interface L_s is illustrated in Fig. 7. We take the tangent to the interface curve; the distance between the two-intersection points is the width of the diffuse interface. Taking nC_4 as an example, at temperature $T = 333.28$ K, $F(n) - F_0(n_{\text{init}}) \cong 2.7306 \times 10^{-18}$ J. Here, in our numerical experiment, the volume of the drop V is $(0.4 \times L)^3$. Along with the radius r_{3D} , we can get the surface area of the droplet $\tilde{A} = 4\pi \times (r_{3D} + L_s/2)^2$ based on the diffuse interface theory. Then, the surface tension is calculated as $\sigma = 2.7306 \times 10^{-18} / \tilde{A} = 6.543 \times 10^{-3} \text{ J/m}^2 = 6.543 \text{ mN/m}$. In the same way, the surface tensions of nC_4 and C_3 at other temperatures can also be calculated. The comparisons of the numerical results with the experimental data [57] are depicted in Fig. 8. It can be seen that the differences between the predicted values and the laboratory data in reference [57] are totally less than 5%. However, the predicted values in Ref. [18], which are computed from simulations in two-dimensional space and without considering the width of the two-phase interface, are much larger than the predicted values from the three-dimensional simulations in this paper.

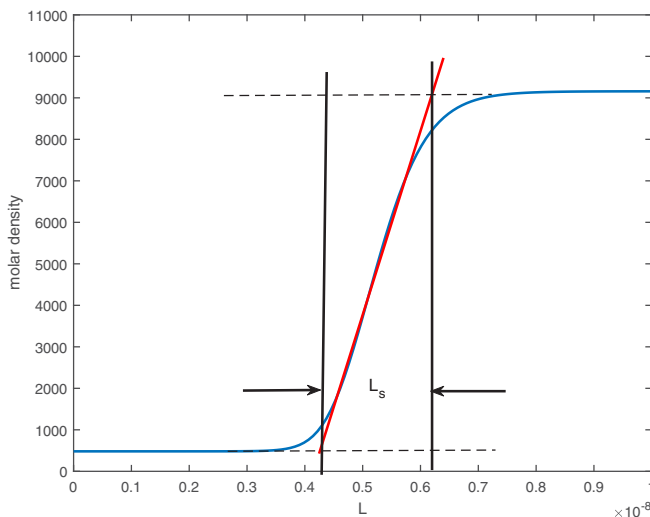


FIG. 7. The width of the diffuse interface.

Next, we will compare our numerical results with the Young-Laplace equation. For the three-dimensional simulation, if we assume that the gas bubble has a spherical shape of radius r ,

$$dA = 8\pi r dr, \quad dV = 4\pi r^2 dr. \quad (45)$$

Combining the above equations, the capillary P_c related to the surface tension σ , can be written in the following well known Young-Laplace equation [1],

$$P_l - P_g = P_c = \sigma dA/dV = 2\sigma/r, \quad (46)$$

where P_l is the pressure in the center of liquid drop [picked from element (100,100,100)], while P_g is the pressure in the bulk gas region [picked from element (50,50,50)]. Here, the thermodynamic pressure of the P-R EOS for the liquid P_l and gas P_g is defined as follows:

$$P_{(l \text{ or } g)} = \frac{nRT}{1 - bn} - \frac{n^2 a(T)}{1 + 2bn - b^2 n}, \quad (47)$$

where the values of parameters $a(T)$ and b could be found in Tables II–IV. Similarly, we take nC_4 as an example. At $T = 333.28$ K, the surface tension $\sigma = 6.543 \times 10^{-3} \text{ N/m}$. The initial droplet radius r is $4.9628 \times 10^{-9} \text{ m}$, while the final droplet radius r^* is about $5.7128 \times 10^{-9} \text{ m}$, and thus, $\sigma/r^* = 1.1453 \text{ Mpa}$. In our numerical results, $P_l = 2.8525 \text{ Mpa}$ and $P_g = 0.5317 \text{ Mpa}$. The difference between them is the capillary pressure $P_c = 2.3208 \text{ Mpa}$. Clearly, the pressure differences computed from LBM agree well with the results from the Young-Laplace equation. The results of nC_4 and C_3 at other temperatures are shown in Fig. 9, where we can see a linear relationship between pressure difference and temperature.

Remark. Compared with the three-dimensional simulation results of Li *et al.* [23], the surface tension computed by our scheme is closer to the laboratory data because of the involved width of the diffuse interface L_s . In addition, the results calculated by the Young-Laplace equation in Ref. [23] do not match the numerical results because they use the two-dimensional Young-Laplace equation while the numerical experiments are in the three-dimensional case. However, in our work, the correct Young-Laplace formula is used, therefore the capillary pressures predicted by the present simulation agree well with those by Young-Laplace equation.

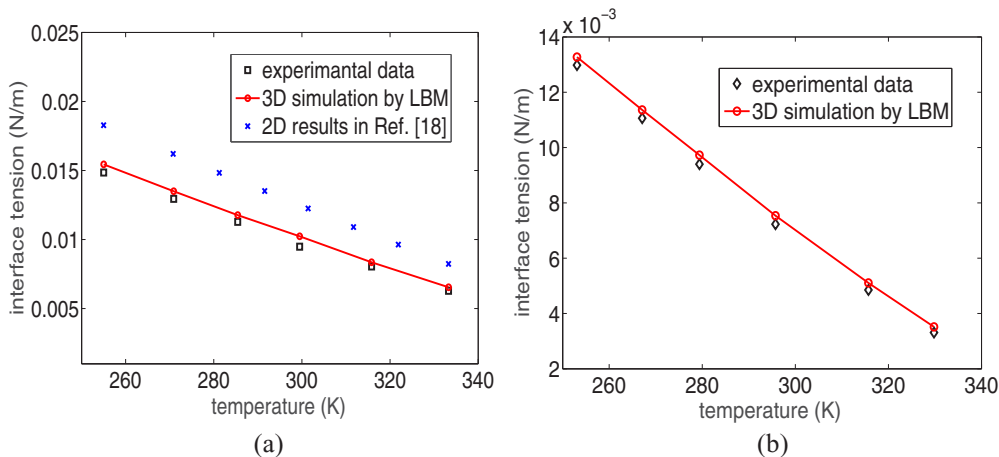


FIG. 8. Comparison of surface tension between numerical predictions and laboratory data; (a) nC_4 , (b) C_3 .

V. CONCLUSION

In this paper, based on the diffuse interface model with P-R EOS, we have proposed a mass conservative LB scheme to simulate realistic two-phase fluid system in three spatial dimensions. Different from the conventional phase field model, a P-R expression of free-energy density rather than double-well form is introduced. Thus, the quantitative modeling of the interface details between different phases can be implemented. The multiscale Chapman-Enskog analysis illustrates that the A-C-type phase equation can be recovered with second order accuracy from the proposed LB scheme. In the mass conservative LB scheme, the Lagrange multiplier is defined based on the mesoscopic character of LBM. It is worth mentioning that this definition way of Lagrange multiplier can be applied to not only periodic boundary conditions but also bounce-back boundaries.

Finally, three-dimensional numerical experiments for real hydrocarbon species, including nC_4 and C_3 , are implemented to test the effectiveness of our proposed LB scheme. Numerical results show that our predictions of surface tension are more accurate than the existing numerical results after considering the width of the two-phase interface.

ACKNOWLEDGMENTS

The authors are grateful to the referees for careful reading and constructive comments that improved the quality of this paper. Z.Q. is partially supported by Hong Kong Research Council GRF Grant No. 15325816. X.Y. is partially supported by the Natural Science Foundation of China (Grant No. 11626095) and the Hong Kong Polytechnic University Postdoctoral Fellowships Scheme 1-YW1D.

APPENDIX

The definition of parameters $a(T)$ and b are given by the following mixing rules [18,19]:

$$a(T) = \sum_{i=1}^M \sum_{j=1}^M y_i y_j (a_i a_j)^{1/2} (1 - k_{ij}), \quad b = \sum_{i=1}^M y_i b_i,$$

where $y_i = n_i/n$ is the mole fraction of component i , k_{ij} is the binary interaction coefficient of P-R EOS, which is usually computed from experimental correlation. The P-R parameters

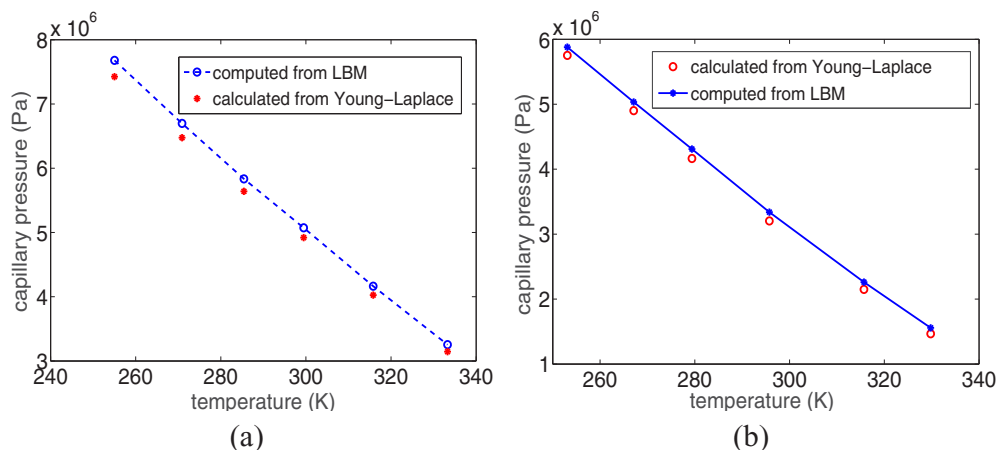


FIG. 9. Comparison with Laplace law: (a) nC_4 , (b) C_3 .

a_i and b_i for pure-substance component i can be derived from the critical properties of the particular species as follows:

$$a_i(T) = 0.45724 \frac{R^2 T_{c_i}^2}{P_{c_i}} \left(1 + m_i \left(1 - \sqrt{\frac{T}{T_{c_i}}} \right) \right)^2,$$

$$b_i = 0.07780 \frac{R T_{c_i}}{P_{c_i}}.$$

Here, T_{c_i} and P_{c_i} represent the critical temperature and the critical pressure of a pure substance, respectively. The parameter m_i has the following relations with the acentric parameter ω_i :

$$m_i = 0.37464 + 1.54226\omega_i - 0.26992\omega_i^2, \quad \omega_i \leq 0.49,$$

$$m_i = 0.379642 + 1.485030\omega_i - 0.164423\omega_i^2$$

$$+ 0.016666\omega_i^3, \quad \omega_i > 0.49.$$

The acentric parameter ω_i can be computed by using critical temperature T_{c_i} , critical pressure P_{c_i} , and the normal boiling

point T_{b_i} :

$$\omega_i = \frac{3}{7} \left[\frac{\log_{10} \left(\frac{P_{c_i}}{14.695 \text{PSI}} \right)}{\frac{T_{c_i}}{T_{b_i}} - 1} \right] - 1.$$

The cross influence parameter c_{ij} can be obtained by using the modified geometric mean rule,

$$c_{ij} = (1 - \beta_{ij}) \sqrt{c_i c_j},$$

where β_{ij} represents the binary interaction coefficient for the influence parameter. Its value is usually assumed to be zero in most engineering practice. c_i is the pure component influence parameter, which is related to the P-R parameters a_i and b_i by [58]

$$c_i = a_i b_i^{2/3} \left(m_{1,i}^c \left(1 - \frac{T}{T_{c_i}} \right) + m_{2,i}^c \right),$$

here, $m_{1,i}^c$ and $m_{2,i}^c$ denote the coefficients which can be related to the acentric factor ω_i by

$$m_{1,i}^c = -\frac{10^{-16}}{1.2326 + 1.3757\omega_i}, \quad m_{2,i}^c = \frac{10^{-16}}{0.9051 + 1.5410\omega_i}.$$

-
- [1] A. Firoozabadi, *Thermodynamics of Hydrocarbon Reservoirs* (McGraw-Hill, New York, 1999).
- [2] L. W. Lake, *Enhanced Oil Recovery* (Prentice-Hall, Englewood Cliffs, NJ, 1989).
- [3] S. Sun and M. F. Wheeler, *SIAM J. Numer. Anal.* **43**, 195 (2005).
- [4] C. Dawson, S. Sun, and M. F. Wheeler, *Comput. Methods Appl. Mech. Eng.* **193**, 2565 (2004).
- [5] J. Moortgat, S. Sun, and A. Firoozabadi, *Water Resour. Res.* **47**, W05511 (2011).
- [6] H. T. Davis, *Statistical Mechanics of Phases, Interfaces, and Thin Films* (VCH, New York, 1996).
- [7] D. Frenkel and B. Smit, *Understanding Molecular Simulation: From Algorithms to Applications* (Academic Press, San Diego, CA, 2001).
- [8] K. B. Haugen and A. Firoozabadi, *J. Chem. Phys.* **130**, 064707 (2009).
- [9] M. Sussman, P. Smereka, and S. Osher, *J. Comput. Phys.* **114**, 146 (1994).
- [10] S. Unverdi and G. Tryggvason, *J. Comput. Phys.* **100**, 25 (1992).
- [11] D. M. Anderson, G. B. McFadden, and A. A. Wheeler, *Annu. Rev. Fluid Mech.* **30**, 139 (1998).
- [12] D. Jacqmin, *J. Comput. Phys.* **155**, 96 (1999).
- [13] J. Kim, *Commun. Comput. Phys.* **12**, 613 (2012).
- [14] Z. Qiao, Z. Sun, and Z. Zhang, *Math. Comp.* **84**, 653 (2015).
- [15] J. Shen and X. Yang, *SIAM J. Sci. Comput.* **32**, 1159 (2010).
- [16] J. Shen and X. Yang, *SIAM J. Sci. Comput.* **36**, B122 (2014).
- [17] Z. Zhang and Z. Qiao, *Commun. Comput. Phys.* **11**, 1261 (2012).
- [18] Z. Qiao and S. Sun, *SIAM J. Sci. Comput.* **36**, B708 (2014).
- [19] X. Fan, J. Kou, Z. Qiao, and S. Sun, *SIAM J. Sci. Comput.* **39**, B1 (2017).
- [20] Q. Peng, *Adv. Appl. Math. Mech.* **9**, 1162 (2017).
- [21] Q. Peng, Z. Qiao, and S. Sun, *J. Comp. Math.* **35**, 737 (2017).
- [22] X. Yang, *J. Comput. Phys.* **327**, 294 (2016).
- [23] H. Li, L. Ju, C. Zhang, and Q. Peng, *J. Sci. Comput.* **75**, 993 (2018).
- [24] J. Kou and S. Sun, *J. Comput. Phys.* **318**, 349 (2016).
- [25] C. Aidun and J. Clausen, *Annu. Rev. Fluid Mech.* **42**, 439 (2010).
- [26] S. Chen and G. Doolen, *Annu. Rev. Fluid Mech.* **30**, 329 (1998).
- [27] Z. Guo and C. Shu, *Lattice Boltzmann Method and Its Applications in Engineering* (World Scientific Publishing, Singapore, 2013).
- [28] A. K. Gunstensen, D. H. Rothman, S. Zaleski, and G. Zanetti, *Phys. Rev. A* **43**, 4320 (1991).
- [29] X. Shan and H. Chen, *Phys. Rev. E* **47**, 1815 (1993).
- [30] X. Shan and H. Chen, *Phys. Rev. E* **49**, 2941 (1994).
- [31] M. R. Swift, E. Orlandini, W. R. Osborn, and J. M. Yeomans, *Phys. Rev. E* **54**, 5041 (1996).
- [32] M. R. Swift, W. R. Osborn, and J. M. Yeomans, *Phys. Rev. Lett.* **75**, 830 (1995).
- [33] L. S. Luo, *Phys. Rev. Lett.* **81**, 1618 (1998).
- [34] L. S. Luo, *Phys. Rev. E* **62**, 4982 (2000).
- [35] X. He, S. Chen, and R. Zhang, *J. Comput. Phys.* **152**, 652 (1999).
- [36] T. Lee and C. L. Lin, *J. Comput. Phys.* **206**, 16 (2005).
- [37] T. Lee and L. Liu, *J. Comput. Phys.* **229**, 8045 (2012).
- [38] H. W. Zheng, C. Shu, and Y. T. Chew, *J. Comput. Phys.* **218**, 353 (2006).
- [39] Q. Li, K. H. Luo, Y. J. Gao, and Y. L. He, *Phys. Rev. E* **85**, 026704 (2012).
- [40] Y. Wang, C. Shu, H. B. Huang, and C. J. Teo, *J. Comput. Phys.* **280**, 404 (2015).
- [41] Y. Wang, C. Shu, J. Y. Shao, J. Wu, and X. D. Niu, *J. Comput. Phys.* **290**, 336 (2015).
- [42] K. Yang and Z. Guo, *Phys. Rev. E* **93**, 043303 (2016).
- [43] Y. Q. Zu and S. He, *Phys. Rev. E* **87**, 043301 (2013).
- [44] L. Zheng, S. Zheng, and Q. Zhai, *Phys. Rev. E* **91**, 013309 (2015).
- [45] S. Ansumali and I. V. Karlin, *Phys. Rev. E* **62**, 7999 (2000).

- [46] I. V. Karlin, A. N. Gorban, S. Succi, and V. Boffi, *Phys. Rev. Lett.* **81**, 6 (1998).
- [47] I. V. Karlin, A. Ferrante, and H. C. Öttinger, *Europhys. Lett.* **47**, 182 (1999).
- [48] A. Mazloomi M, S. S. Chikatamarla, and I. V. Karlin, *Phys. Rev. Lett.* **114**, 174502 (2015).
- [49] A. Mazloomi M, S. S. Chikatamarla, and I. V. Karlin, *Phys. Rev. E* **92**, 023308 (2015).
- [50] A. Mazloomi M, S. Chikatamarla and I. V. Karlin, *Phys. Fluids* **28**, 022106 (2016).
- [51] F. Bösch, B. Dorschner, and I. Karlin, *Europhys. Lett.* **122**, 14002 (2018).
- [52] F. Qin, A. Mazloomi, Q. Kang, D. Derome, and J. Carmeliet, *Phys. Fluids* **30**, 032104 (2018).
- [53] D. Y. Peng and D. B. Robinson, *Ind. Eng. Chem. Fund.* **15**, 59 (1976).
- [54] B. C. Shi and Z. L. Guo, *Phys. Rev. E* **79**, 016701 (2009).
- [55] Y. H. Qian, D. D'Humières, and P. Lallemand, *Europhys. Lett.* **17**, 479 (1992).
- [56] L. Q. Chen and J. Shen, *Comput. Phys. Commun.* **108**, 147 (1998).
- [57] H. Lin and Y.-Y. Duan, *J. Chem. Eng. Data* **48**, 1360 (2003).
- [58] B. Breure and C. J. Peters, *Fluid Phase Equilib.* **334**, 189 (2012).